IIETA International Information and Engineering Technology Association
Advancing the World of Information and Engineering

Journal Européen des Systèmes Automatisés
Vol. 59, No. 3, March, 2026, pp. 729-738
Journal homepage: http://iieta.org/journals/jesa

Performance Analysis of Massive MIMO Systems in Time-Selective Fading Using the Proposed MMSE and EA-MMSE Receiver

B.Ch. Kiran Patrudu[1,2*], P.V.Sridevi[1]

[1] Department of ECE, A.U. College of Engineering, Andhra University, Visakhapatnam 530003, India
[2] Department of ECE, ANITS(A), Visakhapatnam, 531162, India

Corresponding Author Email: bkpatrudu.rs@andhrauniversity.edu.in

https://doi.org/10.18280/jesa.590316

Received: 4 January 2026
Revised: 1 March 2026
Accepted: 9 March 2026
Available online: 31 March 2026

Keywords:
massive multiple-input multiple-output, spectral efficiency, time-selective fading, Imperfect channel state information, Kalman filter

ABSTRACT

Massive multiple-input multiple-output (MIMO) is an essential technology for future wireless systems due to its capability of achieving high spectral efficiency with multiple user support. However, its performance relies on accurate channel state information (CSI), which becomes inconsistent in time-varying environments due to channel aging. This degradation notably affects traditional linear detection schemes, including maximum ratio combining (MRC), zero-forcing (ZF), and Minimum Mean Square Error (MMSE). To address this challenge, the current work proposes an Error-Aware MMSE (EA-MMSE) receiver that explicitly incorporates the channel estimation error covariance into the combining process, allowing enhanced robustness under imperfect CSI. Closed-form expressions for spectral efficiency are obtained for all receivers under both perfect and imperfect CSI. A detailed simulation framework incorporating spatial correlation, shadowing, pathloss modelling, and autoregressive fading validates the analytical results. Numerical evaluations demonstrate that the proposed EA-MMSE consistently attains greater spectral efficiency, especially in conditions of significant channel ageing, making it a promising candidate for practical time-selective massive MIMO deployments.

1. INTRODUCTION

Massive multiple-input multiple-output (MIMO) has emerged as one of the key technologies for 5G and future 6G wireless communication systems due to its ability to serve many users using large antenna arrays at the base station (BS). By exploiting spatial multiplexing and favorable propagation, massive MIMO significantly improves spectral efficiency and energy efficiency compared with conventional multi-antenna systems [1-3]. The primary benefit of massive MIMO lies in its ability to utilize favorable propagation and channel hardening, where random fluctuations in the channel average out as the array size grows, resulting in deterministic equivalent signal-to-interference-plus-noise ratio (SINR) expressions in optimal conditions [4]. However, the achievable performance of massive MIMO fundamentally depends on the availability of accurate channel state information (CSI). In practical communication systems, CSI is estimated via uplink pilot signaling and reused during subsequent data transmission intervals. In rapidly changing propagation environments, particularly with user mobility, Doppler spread, or dynamic scattering, the wireless channel evolves between estimation and use, leading to acquired CSI being outdated —known as channel aging or time-selective fading [5-8]. The ability of linear receivers to suppress interference deteriorates when CSI becomes outdated, and the massive MIMO spatial multiplexing gain cannot be fully realized. For reliable performance in modern mobile systems, the effects of channel aging must be mitigated. Several studies have investigated the impact of channel aging in massive MIMO systems. Auto Regressive (AR) models are widely adopted to characterize channel evolution, while Kalman filtering techniques are employed for channel tracking and prediction. [9-14]. In order to increase resilience to imperfect CSI, parallel research has examined reliable and uncertainty-aware receiver and precoding designs that specifically incorporate error statistics [15-17]. To address CSI inaccuracy and channel dynamics, machine-learning-driven strategies like deep unfolding and reinforcement learning-based precoders have also recently been put forth [18, 19]. Although these works highlight the significance of ageing-aware and imperfect-CSI-robust designs, many of them focus on downlink systems, abstract error models, or do not analyse classical linear receivers under unified theoretical and simulation frameworks. A key reference that forms the foundation of the present research is the work analysed uplink massive MIMO over time-selective fading channels using an AR (1) model and Kalman-filtered CSI [19]. Those results provided theoretical capacity bounds and simulation validation for maximum ratio combining (MRC) and zero-forcing (ZF) receivers under imperfect channel estimation induced by aging. In particular, three important limitations exist in the existing literature. The Minimum Mean Square Error (MMSE) Receiver usually outperforms MRC, ZF receiver under limited interference conditions has not been analysed under time-selective fading environments. A lot of

research evaluates receiver performance only under imperfect CSI without benchmarking the ideal-perfect CSI scenario, making it difficult to quantify the performance degradation caused by channel aging. The estimation error covariance produced by Kalman filtering is not explicitly included in the receiver design. This paper develops a thorough analysis and improvement of uplink massive MIMO under time-selective fading driven by these gaps. First, the prior framework is extended by using the MMSE receiver in addition to MRC and ZF schemes. Second, the degradation caused by aging and estimation error is investigated for both perfect CSI and Kalman-based imperfect CSI for each receiver. Third, and perhaps, a novel Error-Aware MMSE (EA-MMSE) receiver is proposed that explicitly includes the Kalman estimation error covariance into the receive combining matrix. The suggested EA-MMSE actively utilizes the structured error statistics discovered during Kalman tracking, in contrast to the traditional MMSE detector, which views estimation uncertainty as white Gaussian noise. This makes the receiver better suited to time-varying channels where temporal correlation and recursive estimation produce non-white estimation errors. To evaluate and validate the proposed architecture, the closed-form spectral efficiency expressions for MRC, ZF, MMSE, and EA-MMSE under both CSI assumptions are derived. Also, the results showed that the proposed EA-MMSE consistently outperforms its conventional counterpart, especially under severe channel aging, low pilot overhead, and high mobility conditions, offering substantial gains in spectral efficiency without prohibitive computation cost.

2. SYSTEM MODEL AND RECEIVER PROCESSING

Consider the uplink of a single-cell massive MIMO system with a BS equipped with M antennas and K single-antenna user terminals, as illustrated in Figure 1. Communication is assumed to operate in TDD mode so that the uplink and downlink share the same channel response within a coherence interval. The overall system model, including the channel estimation stage and different linear receivers (MRC, ZF, MMSE, and the proposed EA-MMSE), is shown in Figure 1. Due to user mobility and Doppler, the small-scale fading is time-selective, and channel coefficients evolve from symbol time t−1 to t with a temporal correlation factor α ($0 < \alpha \leq 1$). The received signal at the BS during a data symbol interval is modelled as a linear superposition of the user signals plus additive noise. Specifically, if y[t] denotes the M×1 vector of samples collected by the BS antennas at time t, then the received vector is written as

$$y[t] = \sqrt{P_u} G[t] \times [t] + n[t] \quad (1)$$

where, y[t] is the received signal vector at the BS of order Mx1, P_u is the uplink transmit power per user, $x[t] = [x_1[t] \dots \dots . x_K[t]^T]$ is the Kx1 transmit symbol vector with $E\{|x_K[t]|^2\} = 1$. $G[t] = [g_1[t] \dots \dots . g_K[t]] \in \mathbb{C}^{M\times K}$ is the time-varying uplink channel matrix. $n[t] \in \mathbb{C}^{M\times 1}$ is AWGN with i.i.d entries $n_m[t] \sim \mathbb{C}\mathcal{N}(0,1)$. The m, k-th element $g_{mk}[t]$ of G[t] is modelled as the product of small-scale fading and large-scale fading,

$$g_{mk} = h_{mk}\sqrt{\beta_k}, m = 1,2, \dots \dots M, k = 1,2, \dots \dots K \quad (2)$$

where, β_k captures geometric attenuation and shadow fading for user k, and h_{mk} denotes the fast-fading coefficient of order MxK. As in standard massive MIMO analysis,

$$G[t] = H[t]D^{1/2} \quad (3)$$

where, $H[t] \in \mathbb{C}^{M\times K}$ contains i.i.d entries $h_{mk}[t] \sim \mathbb{C}(0,1)$ and $D^{1/2} = \text{diag}(\sqrt{\beta_1}, \sqrt{\beta_2}, \dots \dots \sqrt{\beta_K})$.

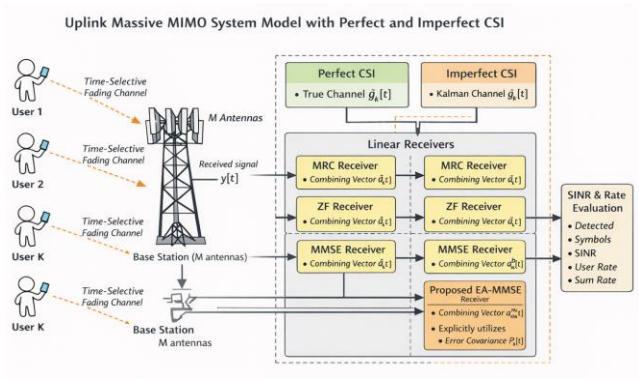

Figure 1. Block diagram of uplink massive multiple-input multiple-output (MIMO) with channel estimation and linear receivers

2.1 Time-selective fading: AR (1) aging model and Kalman filtering

To capture time selectivity, an AR (1) (Jakes-like) evolution for the small-scale fading is adopted for each m,k,

$$h_{mk}[t] = \alpha h_{mk}[t-1] + \sqrt{1-\alpha^2} z_{mk}[t] \quad (4)$$

where, $z_{mk}[t] \sim \mathbb{C}(0,1)$ are i.i.d over (m,k,t) and independent of $h_{mk}[t-1]$. The parameter α represents the temporal correlation between two consecutive symbols; α tends to 1, corresponding to slow fading (quasi-static channel), whereas a smaller α corresponds to faster time variations. In vector form, the user-specific channel vector for each k is defined as

$$g_k[t] = [\, g_{1k}[t] \dots \dots . g_{Mk}[t]]^T \in \mathbb{C}M \times 1 \quad (5)$$

and write the time-selective evolution as

$$g_k[t] = \alpha g_k[t-1] + \sqrt{1-\alpha^2} q_k[t] \quad (6)$$

where, $q_k[t] \sim \mathbb{C}(0, \beta_k I_M)$. Eqs. (1-6) together define the time-selective uplink massive MIMO system model.

2.2 Pilot transmission and Kalman-based channel tracking (imperfect channel state information)

Within each coherence interval, a portion of the time is reserved for uplink pilot transmission. Let T denote the coherence block length (in symbols) and τ be the length of the pilot phase ($\tau \geq K$). For simplicity, the index blocks are denoted by i = 1, 2, …, and the pilot time within block i by $t = t_i^{pilot}$ and data symbols by $t \in \tau_i^{data}$. During the pilot phase of block i, all K users simultaneously transmit mutually orthogonal pilots of length τ. The pilot sequences are collected into a τ × K matrix. $\sqrt{P_P}\phi$ with $\phi^H\phi = I_K$, where $P_P = \tau P_u$

is the pilot power. The received pilot matrix at the BS is

$$Y_p[i] = \sqrt{P_P} G[i]\phi^T + N_p[i] \quad (7)$$

where, $G[i] \triangleq G[t_i^{pilot}]$ and $N_p[i] \in \mathbb{C}^{M\times\tau}$ has i.i.d $\mathbb{C}\mathcal{N}$ (0,1) entries.

Using Eq. (7), an MMSE estimate of the channel matrix at the start of block i is obtained as [4]:

$$\hat{G}[i|i] = \frac{1}{\sqrt{P_P}} Y_p[i]\phi^* \tilde{D} \quad (8)$$

where,

$$\tilde{D} = (\frac{1}{P_P} D^{-1} + I_K)^{-1} \quad (9)$$

The estimation error matrix is defined as

$$E[i] \triangleq \hat{G}[i|i] - G[i] \quad (10)$$

For each user k, the elements of the error column $\varepsilon_k[i|i]$ are zero-mean complex Gaussian with variance

$$\sigma^2{}_{e,k} = \frac{\beta_k}{P_P\beta_k + 1} \quad (11)$$

By MMSE properties, E[i|i] is independent of $\hat{G}[i|i]$. Because the channel is time-selective, the estimate at the start of a block is propagated in time using the AR (1) model and Kalman filtering. For each user k, the prediction step from block i to a later symbol time $t \in \tau_i^{data}$ is

$$\widehat{g_k}[t|i] = \alpha^{\Delta_t}\widehat{g_k}[i|i] \quad (12)$$

With $\Delta_t = t - t_i^{pilot}$ and the prediction error covariance becomes

$$P_k[t|i] = \alpha^{2\Delta_t} P_k[i|i] + (1 - \alpha^{2\Delta_i})\beta_k I_M \quad (13)$$

where, $P_k[i|i] = E\{e_k[i|i]e_k{}^H[i|i]\}$ and $e_k = \varepsilon_k$. In compact form, we denote the time-indexed estimate and error as a

$$G[t] = \hat{G}[t] + E[t], \quad t \in \tau_i^{data} \quad (14)$$

This state-space model Eqs. (1)-(6) together with Eqs. (7)-(14) defines the imperfect CSI with Kalman tracking used in the proposed analysis.

3. LINEAR RECEIVERS AND ACHIEVABLE SUM RATE

The BS applies a linear detector (receiver) to separate the K users. At each time t, the BS constructs a detector matrix $A[t] \in \mathbb{C}^{MxK}$ whose columns correspond to combining vectors for each user. The post-combining signal vector is

$$r[t] = A^H[t]y[t] \quad (15)$$

Expressions for perfect CSI and imperfect CSI are derived separately, followed by specific forms for MRC, ZF, MMSE, and the proposed EA-MMSE receiver.

3.1 Perfect channel state information case

When perfect CSI is available, the detector matrix $A_P[t]$ is designed directly from the true channel G[t]. Substituting Eqs. (1) into (15), we obtain

$$r_P[t] = \sqrt{P_u} A_P{}^H[t]G[t]x[t] + A_P{}^H[t]n[t] \quad (16)$$

Let $a_{k,P}[t]$ be the k-th column of $A_P[t]$ and $g_k[t]$ be the k-th column of G[t]. The scalar output for user k is defined as below:

$$r_{k,P}[t] = \sqrt{P_u} a_{k,P}{}^H[t]g_k[t]x_k[t] + \sqrt{P_u}\sum_{i=1,i\neq k}^{K} a_{k,P}{}^H[t]g_i[t]x_i[t] + a_{k,P}{}^H[t]n[t] \quad (17)$$

The first term in Eq. (17) is the desired signal, the second term is multi-user interference, and the third is filtered noise. Treating the interference as Gaussian noise, the instantaneous SINR at time t for user k under perfect CSI and general linear detection is

$$\gamma_{k,P}[t] = \frac{P_u\left|a_{k,P}{}^H[t]g_k[t]\right|^2}{P_u\sum_{i=1,i\neq k}^{K}\left|a_{k,P}{}^H[t]g_i[t]\right|^2 + \left\|a_{k,P}[t]\right\|^2} \quad (18)$$

The ergodic achievable rate for user k is then

$$R_{k,P} = E\{log_2(1 + \gamma_{k,P}[t])\} \quad (19)$$

And the sum rate per cell is

$$R_{sum,P} = \sum_{k=1}^{K} R_{k,P} \quad (20)$$

Let us now specify $A_P[t]$ for the different linear receivers.

3.1.1 Maximum ratio combining with perfect channel state information

For MRC, the BS uses the channel itself as the combining matrix,

$$A_P{}^{MRC}[t] = G[t] \quad (21)$$

Thus $a_{k,P}[t] = g_k[t]$. Substituting into Eq. (18)

$$\gamma_{k,P}{}^{MRC}[t] = \frac{P_u\|g_k[t]\|^4}{P_u\sum_{i=1,i\neq k}^{K}|g_k{}^H[t]g_i[t]|^2 + \|g_k[t]\|^2} \quad (22)$$

The corresponding rate $R_{k,P}{}^{MRC}$ is obtained by substituting Eqs.(22) into (19).

3.1.2 A large-M closed-form bound for maximum ratio combining (perfect channel state information)

Under i.i.d Rayleigh fading, $g_k[t] \sim \mathbb{C}\mathcal{N}(0, \beta_k I_M)$

The squared norm of the channel vector follows a Chi-square distribution with 2M degrees of freedom, which leads to

$$\mathrm{E}\{\|g_k[t]\|^2\} = \mathrm{M}\beta_k \tag{23}$$

Similrly cross correlation terms between independent user channels satisfy

$$\mathrm{E}\{\|g_k[t]\|^4\} = {\beta_k}^2(M^2 + M) \tag{24}$$

$$\mathrm{E}\{|{g_k}^H[t]g_i\,[t]|^2\} = M\beta_k\beta_i, \qquad i \neq k \tag{25}$$

Substituting these expectations into Eq. (22) yields the large-M approximation.

$$\begin{aligned} {\gamma_{(k,P)}}^{MRC}[t] &\approx \frac{P_u M^2 {\beta_k}^2}{P_u M\beta_k \sum_{i=1,i\neq k}^{K}\beta_I + M\beta_k} \\ &= \frac{P_u M\beta_k}{P_u \sum_{i=1,i\neq k}^{K}\beta_I + 1} \end{aligned} \tag{26}$$

3.1.3 Zero-forcing with perfect channel state information

For ZF, the combining matrix is chosen to eliminate intra-cell interference:

$${A_P}^{ZF}[t] = G[t](G^H[t]G[t])^{-1} \tag{27}$$

This choice ensures

$${A_P}^{ZF,H}[t]G[t] = I_K, \qquad \Rightarrow {a_{k,P}}^H[t]g_i[t] = \delta_{ki} \tag{28}$$

Substituting Eqs. (28) into (18) gives the ZF SINR

$${\gamma_{k,P}}^{ZF}[t] = \frac{P_u}{\left\|{a_{k,P}}^{ZF}[t]\right\|^2} = \frac{P_u}{[(G^H[t]G[t])^{-1}]_{kk}} \tag{29}$$

Again, the rate ${\mathrm{R}_{k,P}}^{ZF}$ follows from Eq. (19)

3.1.4 A large-M closed-form bound for zero-forcing (perfect channel state information)

For i.i.d. Rayleigh fading, the Gram matrix. $G^H[t]\,G[t]$ is central Wishart with M degrees of freedom and covariance D = diag($\beta_1, \beta_2, \ldots \ldots \beta_M$). A standard result gives, for large M,

$$\mathrm{E}\{[(G^H[t]G[t])^{-1}]_{kk}\} \approx \frac{1}{(M-K)\beta_k}. \tag{30}$$

Substituting this approximation into Eq. (25) yields the closed-form large-M SINR bound.

$${\gamma_{(k,P)}}^{ZF}[t] \approx P_u(M-K)\beta_k \tag{31}$$

3.1.5 Minimum Mean Square Error with perfect channel state information

For the MMSE receiver with perfect CSI, the combining matrix is chosen as

$${A_P}^{MMSE}[t] = (G[t]G^H[t] + \frac{1}{P_u}I_M)^{-1}G[t] \tag{32}$$

The k-th combining vector can be expressed in the equivalent scalar form as

$$\begin{aligned} {a_{k,P}}^{MMSE}[t] = {v_k}^{-1}[t]g_k[t]/({g_k}^H[t]{v_k}^{-1}[t]g_k[t] \\ + 1 \end{aligned} \tag{33}$$

where,

$$v_k[t] = \sum_{i=1,i\neq k}^{K} g_i[t]\,{g_i}^H[t] + \frac{1}{P_u}I_M \tag{34}$$

Substituting Eqs. (33) into (18) and simplifying gives the well-known SINR.

$${\gamma_{k,P}}^{MMSE}[t] = {g_k}^H[t]{v_k}^{-1}[t]g_k[t] \tag{35}$$

The rate ${\mathrm{R}_{k,P}}^{MMSE}$ is again obtained from Eq. (19). In the massive MIMO regime, this SINR admits deterministic equivalents and closed-form lower bounds obtained via random matrix theory.

3.1.6 A deterministic-equivalent bound for MMSE (perfect channel state information)

A convenient **analytic bound** for the MMSE receiver is obtained by replacing the random Gram matrix in Eq. (29) by its deterministic equivalent. For i.i.d. Rayleigh fading, the matrix.

$$\frac{1}{M}G^H[t]G[t] \Rightarrow D = \mathrm{diag}(\beta_1, \beta_2, \ldots \ldots \beta_K). \tag{36}$$

As M→∞. inserting this into Eqs. (26) and (29) yields the large-M deterministic-equivalent SINR

$${\gamma_{(k,P)}}^{MMSE}[t] \approx \frac{P_u(M\beta_k)}{1 + \sum_{i=1,i\neq k}^{K}\frac{\beta_i}{1+P_u\beta_i}} \tag{37}$$

3.1.7 Error-Aware Minimum Mean Square Error with perfect channel state information (special case)

The proposed error-aware MMSE receiver explicitly exploits the estimation error covariance. Under perfect CSI, there is no estimation error and, hence, the error covariance matrices are zero. Therefore, the EA–MMSE structure reduces to the conventional MMSE receiver:

- error covariance $P_k[t] = 0$ for all users k and time t
- effective covariance:${V_k}^{EA}[t]=v_k[t]$
- combining vectors: ${a_k}^{EA}[t] = {a_{(k,P)}}^{MMSE}[t]$
- SINR: ${\gamma_{(k,P)}}^{EA}[t] = {\gamma_{(k,P)}}^{MMSE}[t]$

Thus, under perfect CSI, EA–MMSE and MMSE coincide, and the bound (29a) also serves as the EA–MMSE bound.

3.2 Imperfect channel state information with time-selective fading

Considering the practically relevant case where the BS only knows a Kalman-tracked estimate of the time-selective channel. At time t, the true channel can be written as

$$\mathrm{G}\widehat{[\mathrm{t}]} = G[t + \mathrm{E}[\mathrm{t}]] \tag{38}$$

where, $\hat{G}\,[t]$ is the kalman predictor/corrector output and E[t] is the residual estimation error with E{E[t]}=0 and user dependent error variances ${\sigma_{e,k}}^2(\alpha, \tau, P_p)$ that depend on α, pilot length and training SNR. Substituting Eq. (38) into Eq. (1), the received signal becomes

$$y[t] = \sqrt{\mathrm{P_u}}\hat{G}\,[t]x[t] - \sqrt{\mathrm{P_u}}E[t]x[t] + n[t] \tag{39}$$

The BS constructs a detector matrix $\hat{A}\,[t]$ based only on the estimated channel $\hat{G}[t]$. After linear detection,

$$\hat{r}[t] = \hat{A}^{H}[t]y[t] \tag{40}$$

Let $\hat{a}_k[t]$ and $\hat{g}_k[t]$ be the k-th columns of $\hat{A}\,[t]$ and $\hat{G}\,[t]$ respectively and let $\varepsilon_k[t]$ be the k-th error column. The output for user k is:

$$\begin{aligned}&\hat{r}[t]\\&= \sqrt{\mathrm{P_u}}\hat{a}_k{}^{H}[t]\hat{g}_k[t]x_k[t]\sqrt{\mathrm{P_u}}\sum_{i=1,i\neq k}^{K}\hat{a}_k{}^{H}[t]\hat{g}_i[t]x_i[t]\\&-\sqrt{\mathrm{P_u}}\sum_{i=1}^{K}\hat{a}_k{}^{H}[t]\hat{\varepsilon}_i[t]x_i[t]+\hat{a}_k{}^{H}[t]n[t]\end{aligned} \tag{41}$$

In Eq. (41), the terms correspond to the desired signal, residual multi-user interference, estimation-error-induced interference, and filtered noise. Conditioned on $\hat{G}\,[t]$, The effective SINR for user k under imperfect CSI and generic linear detection can be written as:

$$\gamma_{k,I}[t] = \frac{P_u\left|\hat{a}_k{}^{H}[t]\hat{g}_k[t]\right|^2}{P_u\sum_{i=1,i\neq k}^{K}\left|\hat{a}_k{}^{H}[t]\hat{g}_i[t]\right|^2+\mathrm{P_u}\sum_{i=1}^{K}E\{\left|\hat{a}_k{}^{H}[t]\hat{\varepsilon}_i[t]\right|\}^2+\|\,\hat{a}_k[t]\|^2]} \tag{42}$$

Using the error statistics from Eqs. (11-14), the term $E\{\left|\hat{a}_k{}^{H}[t]\hat{\varepsilon}_i[t]\right|\}^2$ reduces to $\sigma_{e,i}{}^2(\alpha)\|\hat{a}_k[t]\|^2$. Thus Eq. (42) becomes:

$$\gamma_{k,I}[t] = \frac{P_u\left|\hat{a}_k{}^{H}[t]\hat{g}_k[t]\right|^2}{P_u\sum_{i=1,i\neq k}^{K}\left|\hat{a}_k{}^{H}[t]\hat{g}_i[t]\right|^2+\mathrm{P_u}\sum_{i=1}^{K}\sigma_{e,i}{}^2(\alpha)\|\,\hat{a}_k[t]\|^2+\|\,\hat{a}_k[t]\|^2]} \tag{43}$$

The ergodic achievable rate and sum rate with imperfect CSI are then:

$$R_{k,P} = (1-\frac{\tau}{T})E\{log_2\big(1+\gamma_{k,I}[t]\big)\} \tag{44}$$

$$R_{sum,I} = \sum_{k=1}^{K}R_{k,I} \tag{45}$$

The pre-factor $(1-\frac{\tau}{T})$ accounts for pilot overhead. Next, the detector matrix $\hat{A}[t]$For different receivers are specified.

3.2.1 Maximum ratio combining with imperfect CSI

For MRC with imperfect CSI, the combining matrix is simply the estimated channel and is given by

$$\hat{A}^{MRC}[\mathrm{t}] = \hat{G}[t], \qquad \hat{a}_k[t] = \hat{g}_k[t] \tag{46}$$

Substituting Eqs. (46) into (43) yields

$$\gamma_{k,I}{}^{MRC}[t] = \frac{P_u\|\hat{g}_k[t]\|^4}{P_u\sum_{i=1,i\neq k}^{K}\left|\hat{g}_k{}^{H}[t]\hat{g}_i[t]\right|^2+\mathrm{P_u}\sum_{i=1}^{K}\sigma_{e,i}{}^2(\alpha)\|\hat{g}_k[t]\|^2+\|\hat{g}_k[t]\|^2]} \tag{47}$$

This expression clearly shows how the time-selective estimation error, through $\sigma_{e,i}{}^2(\alpha)$, degrades the effective SINR.

3.2.2 A large-M closed-form bound for maximum ratio combining (imperfectchannel state information)

Let $\hat{g}_k[t]\sim\mathbb{C}(0,\gamma_k I_M)$ be the MMSE/Kalman estimate of user k's channel with variance γ_k=$\beta_k-\sigma_{e,k}{}^2$. Then

- $\mathrm{E}\{\|\,\hat{g}_k[t]\|^2\}$= $\mathrm{M}\gamma_k$
- $\mathrm{E}\{\|\,\hat{g}_k[t]\|^4\}\approx M^2\gamma_k{}^2$
- $\mathrm{E}\{\left|\hat{g}_k{}^{H}[t]\hat{g}_i[t]\right|^2\}\approx \mathrm{M}\gamma_k\gamma_i,\ i\neq k$
- $\mathrm{E}\{\left|\hat{g}_k{}^{H}[t]\varepsilon_i[t]\right|^2\}\approx \mathrm{M}\gamma_k\sigma_{e,i}{}^2$

Substituting these into Eq. (47) and cancelling the common factor $\mathrm{M}\gamma_k$ yields the large-M SINR bound,

$$\gamma_{k,I}{}^{MRC}[t] = \frac{P_u\mathrm{M}\gamma_k}{P_u\sum_{i=1,i\neq k}^{K}\gamma_i+\mathrm{P_u}\sum_{i=1}^{K}\sigma_{e,i}{}^2+1} \tag{48}$$

3.2.3 Zero-forcing with imperfect channel state information

For ZF with imperfect CSI, the combining matrix is

$$\hat{A}^{ZF}[\mathrm{t}] = \hat{G}[t](\hat{G}^{H}[t]\hat{G}[t])^{-1} \tag{49}$$

By construction, $\hat{A}^{ZF^{H}}[\mathrm{t}]\ \hat{G}[t]=I_K$. So in the estimated domain, there is no inter-user interference:

$$\hat{a}_k{}^{ZF^{H}}[t]\ \hat{g}_i[t]=\delta_{ki} \tag{50}$$

However, due to the presence of E[t], residual interference and self-interference remain. Substituting Eqs. (40)-(41) into Eq. (43), the ZF SINR with imperfect CSI becomes:

$$\begin{aligned}&\gamma_{k,I}{}^{ZF}[t]\\&=\frac{P_u}{\mathrm{P_u}\sum_{i=1}^{K}\sigma_{e,i}{}^2(\alpha)\left\|\hat{a}_k{}^{ZF}[t]\right\|^2+\left\|\hat{a}_k{}^{ZF}[t]\right\|^2}\end{aligned} \tag{51}$$

Equivalently, this can be expressed in terms of the inverse Gram matrix of the estimated channel, showing the impact of both. $\hat{G}[t]$ and the estimation error covariance.

3.2.4 A large-M closed-form bound for zero-forcing (imperfect CSI)

For large M, the squared norm of the ZF combining vector can be approximated as $\left\|\,\hat{a}_k{}^{ZF}[t]\right\|^2\approx\frac{1}{(M-K)\gamma_k}$. Substituting this into Eq. (51) gives:

$$\begin{aligned}\gamma_{k,I}{}^{ZF}[t]&\approx\frac{\mathrm{P_u}}{\frac{\mathrm{P_u}\sum_{i=1}^{K}\sigma_{e,i}{}^2(\alpha)+1}{(M-K)\gamma_k}}\\&=\frac{\mathrm{P_u}(M-K)\gamma_k}{\mathrm{P_u}\sum_{i=1}^{K}\sigma_{e,i}{}^2(\alpha)+1}\end{aligned} \tag{52}$$

Eq. (52) provides a closed-form large-M bound for ZF under imperfect CSI.

3.2.5 Minimum Mean Square Error with imperfect channel state information

For MMSE with imperfect CSI, the receiver must account for both multi-user interference and the extra noise caused by estimation error. A natural choice is to define the effective interference-plus-noise covariance for user k as:

$$\hat{v}_k[t] = P_u \sum_{i=1, i\neq k}^{K} \left|\hat{g}_i[t]\hat{g}_i{}^H[t]\right|^2 + \left(\sum_{i=1}^{K} \sigma_{e,i}{}^2(\alpha) + \frac{1}{P_u}\right) I_M \quad (53)$$

The conventional MMSE detector that uses only $\hat{G}[t]$ then takes

$$\hat{a}_k{}^{MMSE}[t] = \hat{v}_k[t]^{-1}\, \hat{g}_k[t] / (\hat{g}_k{}^H[t]\, \hat{v}_k[t]^{-1}\, \hat{g}_k[t] + 1) \quad (54)$$

Substituting (54) into (43) yields the MMSE SINR under imperfect CSI, which simplifies to

$$\gamma_{k,I}{}^{MMSE}[t] = \hat{g}_k{}^H[t]\, \hat{v}_k[t]^{-1}\, \hat{g}_k[t] \quad (55)$$

This is structurally similar to (35), but with a covariance matrix that now explicitly depends on estimation error statistics through $\sigma_{e,i}{}^2(\alpha)$.

3.2.6 A deterministic-equivalent bound for Minimum Mean Square Error (imperfect channel state information)

By replacing the random Gram matrix in Eq. (53) with its deterministic equivalent and using standard random matrix theory arguments, a large-M analytic bound of the formis obtained.

$$\gamma_{k,I}{}^{MMSE}[t] = \frac{\mathrm{P_u} M \gamma_k}{1 + \mathrm{P_u} \sum_{i=1}^{K} \frac{\gamma_i}{1 + \mathrm{P_u}\gamma_i} + \mathrm{P_u} \sum_{i=1}^{K} \sigma_{e,i}{}^2} \quad (56)$$

The exact expression Eq. (55) is used in Monte Carlo averaging, while Eq. (56) provides a closed-form approximation that underlies the theoretical MMSE curves.

3.2.7 Proposed Error-Aware Minimum Mean Square Error receiver

The key idea behind the proposed EA-MMSE receiver is to explicitly incorporate the channel estimation error covariance obtained from Kalman filtering into the receive combining process. In conventional MMSE detection, the receiver treats channel estimation errors as independent noise and does not exploit their statistical structure. However, in time-selective fading environments, the Kalman filter provides valuable information about the temporal evolution of the channel and the reliability of the estimates. The operation of the EA-MMSE receiver can be understood through the following steps. First, the BS obtains the channel estimates. $\hat{g}_k[t]$ for all users using the Kalman filter described earlier. Along with the channel estimates, the Kalman filter also provides the corresponding estimation error covariance matrices, $P_k[t]$, which capture the uncertainty associated with the estimated channels. Next, these channel estimates and their covariance matrices are used to construct the effective interference-plus-noise covariance matrix. In the proposed EA-MMSE receiver, the time-selective Kalman structure can be exploited by replacing the scalar error variances. $\sigma_{e,i}{}^2(\alpha)$ in Eq. (52) with the full Kalman error covariance. For user k, the prediction/update process gives an error covariance matrix. $P_k[t]$ as in Eq. (13). The effective interference-plus-noise covariance is modelled as

$$V_k{}^{EA}[t] = \sum_{i=1, i\neq k}^{K} \hat{g}_i[t]\hat{g}_i{}^H[t] + \sum_{i=1}^{K} P_i[t] + \frac{1}{P_u} I_M \quad (57)$$

Once this covariance matrix is obtained, the EA-MMSE combining vector is computed to spatially filter the received signal and suppress interference and noise. The EA-MMSE combining vector is defined as:

$$a_k{}^{EA}[t] = (V_k{}^{EA}[t]^{-1}\, \hat{g}_k[t] \,/ (\widehat{g}_k{}^H[t](V_k{}^{EA}[t]^{-1}\, \hat{g}_k[t] + 1)) \quad (58)$$

The combining vector is then applied to the received signal to detect the desired user's data. By substituting Eq. (56) into the general SINR expression Eq. (43), the EA-MMSE SINR becomes

$$\gamma_{k,I}{}^{EA}[t] = \hat{g}_k{}^H[t](V_k{}^{EA}[t])^{-1}\, \hat{g}_k[t] \quad (59)$$

Compared to the conventional MMSE in Eq. (55), the proposed EA-MMSE explicitly incorporates the time-varying error covariance matrices $P_i[t]$, which depend on α, τ, P_p and the Kalman update. This novel awareness of temporal channel dynamics allows the receiver to more accurately weight each BS antenna, improving the achievable sum rate, especially in highly time-selective regimes (small α). Finally, the corresponding user rates $R_{k,I}{}^{EA}$ and the sum rate $R_{sum,I}{}^{EA}$ are obtained by substituting Eq. (49) into Eqs. (36)-(37). These expressions, together with their perfect-CSI counterparts in Eqs. (21)-(29), form the analytical basis for the simulation and theoretical curves you already generated in MATLAB.

3.2.8 A Deterministic-equivalent bound for Error-Aware MMSE

A deterministic equivalent SINR for EA-MMSE is obtained by replacing the random matrices in Eq. (57) with their expectations and using the average Kalman error covariance. $\overline{P_i}$. This yields a bound of the form.

$$\gamma_{k,I}{}^{EA}[t] \approx \hat{g}_k{}^H[t]\Big(\sum_{i=1, i\neq k}^{K} \hat{g}_i[t]\hat{g}_i{}^H[t] + \sum_{i=1}^{K} \overline{P_i} + \frac{1}{P_u} I_M\Big)^{-1} \hat{g}_k[t] \quad (60)$$

4. SIMULATION RESULTS

The simulation takes into account the uplink of a single-cell massive MIMO system in time-division duplex (TDD) mode, where K = 8 single-antenna user terminals are simultaneously served by a BS with M antennas, and the Simulation Parameters are presented in Table 1. To prevent near-field effects, the users are evenly distributed within a circular cell that is modelled as an annular region with minimum and maximum radii of 100 m and 1000 m, respectively. Both distance-dependent pathloss with a pathloss exponent of 3.8 and log-normal shadowing with an 8 dB standard deviation are examples of large-scale fading. An exponential correlation matrix is used to capture antenna correlation when modeling small-scale fading as spatially correlated Rayleigh fading. The channel evolves using a first-order autoregressive (AR(1)) time-selective fading model with temporal correlation coefficient α = 0.99 to take user mobility and Doppler effects into account. Uplink CSI is acquired via pilot-assisted MMSE estimation, followed by Kalman-based channel tracking to

predict channel variations during data transmission. The resulting CSI is therefore imperfect and subject to channel aging. The BS uses linear uplink receivers including MRC, ZF, MMSE and the proposed EA-MMSE detector. The evaluation of the sum spectral efficiency is done using 1000 Monte Carlo simulations and compared with analytically derived lower bounds, while accounting for pilot overhead through an appropriate pre-log factor. Figure 2 illustrates the uplink sum spectral efficiency (SE) as a function of the number of BS antennas M under imperfect CSI with Kalman-based channel tracking, for K = 8 users, uplink transmit power. P_u = 10, and temporal correlation coefficient α = 0.99. As the number of antennas increases, the spectral efficiency improves for all receivers due to the array gain and improved spatial resolution provided by the large antenna array. Both Monte Carlo simulation results and corresponding analytical lower bounds are shown for MRC, ZF, MMSE, and the proposed EA-MMSE receiver. Among the receivers, MRC exhibits the weakest performance as it simply aligns the received signal with the desired user channel without actively suppressing interference from other users. The residual inter-user interference dominates with the increase in the number of users. The ZF receiver significantly improves performance by explicitly nulling the interference components through matrix inversion of the estimated channel Gram matrix. However, residual estimation errors caused by time-selective fading limit ZF's performance. The MMSE receiver further improves SE by jointly considering interference suppression and noise amplification, resulting in a better tradeoff between interference cancellation and noise enhancement. Particularly for moderate-to-large M, the proposed EA-MMSE receiver consistently achieves the highest spectral efficiency matching or slightly surpassing MMSE performance. The tight agreement between simulation curves and analytical lower bounds for all receivers, particularly for large M, validates the accuracy of the derived deterministic approximations and confirms that the theoretical analysis reliably captures the impact of channel aging and estimation errors. Finite-dimensional effects and residual channel correlation are expected to cause minor deviations at smaller antenna sizes.

Table 1. Simulation parameters used in the SIMULATION

S.No.	Simulation Parameter	Value
1	No. of base station (BS) antennas	M = 50-500
2	Number of users	K = 8
3	Pathloss Exponent	3.8
4	Shadowing standard deviation	8dB
5	Temporal Correlation	α = 0.99
6	Pilot Length	τ = K
7	Monte Carlo Runs	1000
8	Antenna Correlation	ρ = 0.8

Overall, the results show that the suggested EA-MMSE receiver successfully mitigates CSI imperfections, achieving strong performance gains without undue computational complexity, whereas conventional linear receivers exhibit noticeable degradation under time-selective fading.

Figure 3 shows the variation of the uplink sum SE with the number of BS antennas M for the MRC, ZF, MMSE, and EA-MMSE receivers under perfect CSI, with parameters K = 8, P_u = 10, α = 0.99, and antenna correlation ρ = 0.8. In this case, the BS has accurate knowledge of the instantaneous channel matrix, which allows the receiver to perform optimal interference suppression. SE increases monotonically with the number of antennas for all receivers due to improved array gain and reduced multiuser interference. Because interference is actively suppressed, ZF and MMSE grow almost linearly while MRC grows more slowly because of residual inter-user interference. MMSE and EA-MMSE have the highest sum SE across all M values, with ZF coming in second. For example, at M = 500, ZF achieves approximately 24.33bits/s/Hz, while MMSE/EA-MMSE provides slightly higher values (~24.47 bits/s/Hz), due to joint interference-plus-noise regularisation. In contrast MRCs sensitivity to inter-user interference in correlated channels is demonstrated by the fact that it only achieves ~16.23 bits/s/Hz at the same M. The theoretical curves closely track the simulation results for ZF and MMSE, validating the accuracy of the analytical approximations. For ZF and MMSE, the theoretical curves closely match the simulation results, confirming that the analytical approximations are accurate.

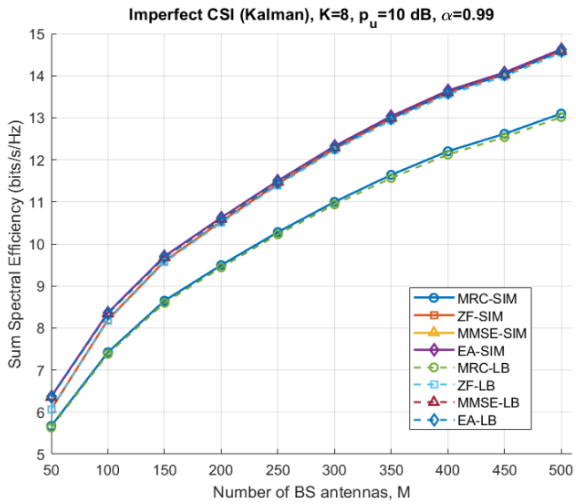

Figure 2. Sum spectral efficiency versus No. of base station (BS) ntennas M for imperfect channel state information (CSI) (K = 8, P_u = 10 dB)

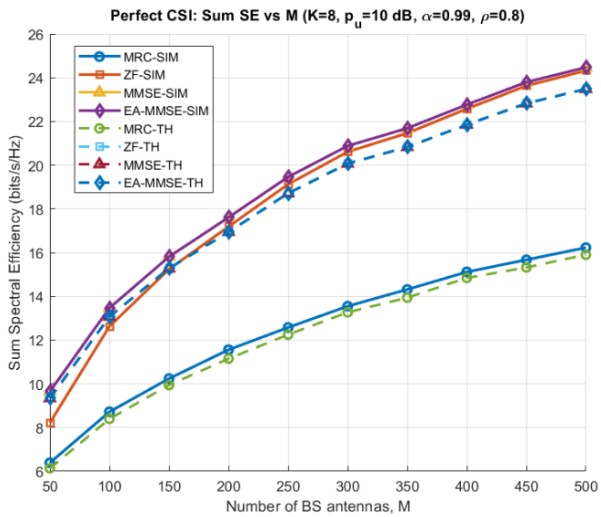

Figure 3. Sum spectral efficiency versus No. of base station (BS) antennas M for Perfect channel state information (CSI) (K = 8, P_u = 10 dB)

Due to spatial correlation and time selectivity, which the simplified theoretical SINR expression does not fully capture, there is still a slight gap for MRC. Overall, the perfect-CSI

results confirm that MMSE/EA-MMSE offers the highest SE, ZF almost matches MMSE under perfect CSI, and MRC performs noticeably worse, especially in correlated settings. These curves serve as the upper performance benchmark against which imperfect-CSI and channel-ageing results can be compared.

The uplink transmit power scales as $P_u(M) = E_u/M^{\gamma}$ with scaling exponents $\gamma = 0.5$ and $\gamma = 1$. Figure 4 examines the uplink power scaling law in a time-selective massive MIMO system under imperfect CSI. When $\gamma = 0.5$, the transmit power decreases as 1/sqrt{M}, and the sum spectral efficiency continues to rise with M for all receivers. This illustrates the traditional massive MIMO result that even in the case of imperfect CSI and channel aging array gain can make up for decreased transmit power.

Among the receivers, MMSE and EA-MMSE consistently attain the highest spectral efficiency, followed by ZF and MRC. When $\gamma = 1$, the transmit power scales as 1/M, the growth of spectral efficiency with M becomes much slower, and in some cases nearly saturates. This behaviour demonstrates the estimation-error-limited regime in which the gains that can be achieved are limited by the dominance of channel estimation errors. Nevertheless, MMSE and EA-MMSE continue to be strong and outperform ZF and MRC in terms of performance.

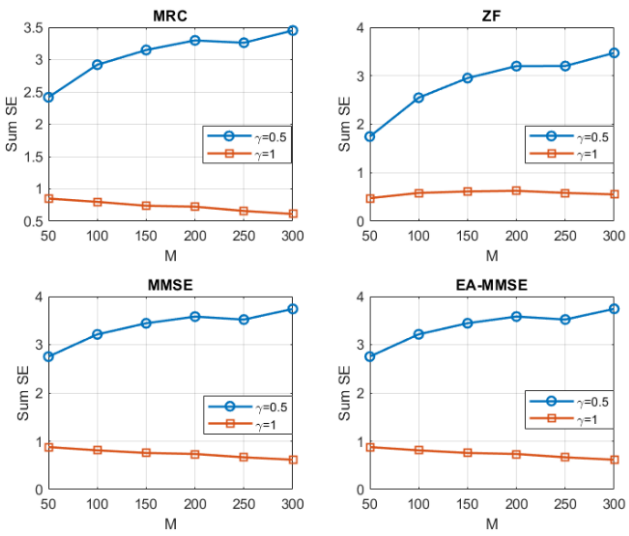

Figure 4. Spectral efficiency vs No. of base station (BS) antennas M for power scaling exponent $\gamma = 0.5$ and $\gamma = 1$ under imperfect channel state information (CSI)

Figure 5 considers the effect of the number of users on the system spectral efficiency. Due to improved spatial multiplexing gains, the sum spectral efficiency first rises with the number of users, reaching a maximum around K≈40–60, it saturates and progressively falls due to the domination of multiuser interference, pilot overhead, and channel estimation errors. Among the receivers, ZF offers a noticeable improvement but becomes more susceptible to CSI imperfections and noise enhancement as K increases, whereas MRC produces the lowest performance and deteriorates rapidly at high user loads because it does not suppress inter-user interference. MMSE outperforms both MRC and ZF by optimally balancing interference suppression and noise amplification, and the proposed EA-MMSE consistently achieves the highest sum spectral efficiency across the entire range of K, particularly in the heavily loaded regime, by explicitly accounting for channel estimation error statistics. Quantitatively, for large K, EA-MMSE provides substantial gains over ZF and noticeable improvements over conventional MMSE, maintaining stable performance where ZF and MRC degrade. These trends also show an optimal user load beyond which the sum spectral efficiency decreases and confirm the superiority of MMSE-type receivers over MRC and ZF; the additional gains observed for EA-MMSE in the high-K regime further demonstrate the effectiveness of error-aware receiver design under practical mobility and correlation conditions.

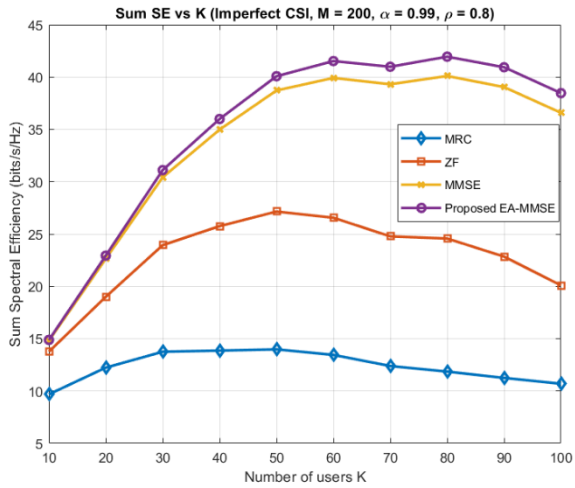

Figure 5. Sum Spectral efficiency versus No. of users K with M = 200, α = 0.99,ρ = 0.8 for imperfect channel state information (CSI)

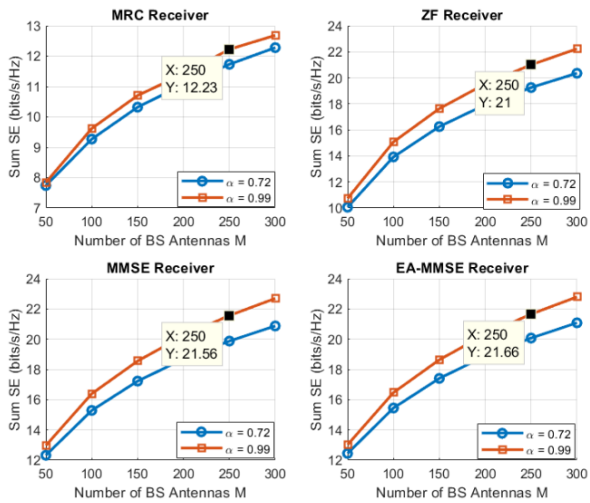

Figure 6. Sum Spectral efficiency versus No. of antennas at BS, M for MRC, ZF, MMSE and EA-MMSE at various values of α = 0.72 and α = 0.99 for imperfect CSI

Note: BS = base station; MRC = maximum ratio combining; ZF = zero-forcing; MMSE = Minimum Mean Square Error; EA-MMSE = Error-Aware MMSE; CSI = channel state information

Figure 6 illustrates how the channel time selectivity affects the uplink sum spectral efficiency in relation to the number of BS antennas M for MRC, ZF, MMSE, and EA-MMSE receivers under imperfect CSI. The favourable propagation and array gain benefits of massive MIMO even in time-selective channels are confirmed by the fact that the sum spectral efficiency increases monotonically with M for all receivers. A higher temporal correlation coefficient (α = 0.99) consistently produces better performance compared to a lower

correlation ($\alpha = 0.72$), since slower channel ageing improves channel tracking accuracy and reduces estimation error.

Among the receivers, MRC exhibits the lowest growth rate with M and the largest sensitivity to channel aging, due to its inability to actively suppress multiuser interference. ZF significantly improves performance by cancelling inter-user interference, but its gain is still limited at lower α because imperfect CSI degrades nulling accuracy. By optimally balancing noise enhancement and interference suppression, MMSE further outperforms ZF across all M, resulting in a steeper increase in sum spectral efficiency. The proposed EA-MMSE achieves the highest performance for both values of α, as it explicitly accounts for channel estimation error covariance, making it more robust to channel aging. The performance gap between $\alpha = 0.72$ and $\alpha = 0.99$ grows with increasing M, especially for MMSE and EA-MMSE, suggesting that accurate temporal correlation modelling becomes increasingly important in large antenna regimes. Overall, the results confirm that higher temporal correlation and error-aware receiver design are critical for fully exploiting massive MIMO gains in time-selective fading environments.

Recent works have also investigated advanced receiver designs for massive MIMO systems, including nonlinear detectors such as successive interference cancellation (SIC), message passing algorithms, and machine-learning-based receivers. While these approaches can provide improved detection performance, they often require significantly higher computational complexity and are less suitable for large-scale antenna systems where low-complexity linear processing is preferred. For this reason, the present work focuses on classical linear receivers such as MRC, ZF, and MMSE, which remain widely adopted in practical massive MIMO deployments due to their scalability and analytical tractability. The proposed EA-MMSE receiver extends this class of linear detectors by incorporating Kalman-based channel estimation error covariance, thereby improving robustness in time-selective fading environments.

4.1 Computational complexity analysis

For practical implementations of Massive MIMO, one of the important aspects is the computational complexity analysis of receiver algorithms, and it depends on the matrix operations to construct the receive combining vectors. The order of complexity is shown in Table 2.

Table 2. Complexity order of receiver algorithms

S.No.	Dominant Operation	Complexity
MRC	Vector inner products	O (MK)
ZF	Gram matrix products	O (K^3)
MMSE	Regularised matrix inversion	O (K^3)
EA-MMSE	Regularised inversion with error covariance	O (K^3)

Note**:** MRC: maximum ratio combining; ZF: zero-forcing; MMSE: Minimum Mean Square Error; EA-MMSE: Error-Aware MMSE

5. CONCLUSION

This paper investigated the uplink performance analysis of massive MIMO systems operating in time-selective fading environments. A unified framework was developed to evaluate the spectral efficiency of linear receivers, including MRC, ZF and MMSE receivers under both perfect and imperfect CSI. The analysis considers practical propagation effects such as spatial correlation, large-scale fading and channel aging. In addition, a novel EA-MMSE receiver is proposed that explicitly incorporates the Kalman estimation error covariance into the receiver combining process. The analytical expressions derived for spectral efficiency were validated through Monte Carlo simulations under realistic propagation conditions, including spatial correlation, pathloss, shadowing, and channel aging. The results demonstrate that channel aging significantly degrades the performance of conventional receivers, particularly when CSI becomes outdated. By exploiting the estimation error statistics, the proposed EA-MMSE receiver achieves improved robustness in time-varying channels while maintaining computational complexity comparable to conventional MMSE detection. Overall, the study highlights the importance of error-aware receiver design and accurate CSI tracking for sustaining spectral efficiency gains in practical massive MIMO systems operating in time-selective fading environments.

REFERENCES

[1] Moerman, A., Van Kerrebrouck, J., Caytan, O., De Paula, I., et al. (2022). Beyond 5G without obstacles: MmWave-over-fiber distributed antenna systems. IEEE Communications Magazine, 60(1): 27-33. https://doi.org/10.1109/MCOM.001.2100550

[2] Marzetta, T.L., Larsson, E.G., Yang, H., Ngo, H.Q. (2023). Fundamentals of Massive MIMO. Cambridge University Press, Cambridge, UK.

[3] Ngo, H.Q., Larsson, E.G., Marzetta, T.L. (2013). Energy and spectral efficiency of very large multiuser MIMO systems. IEEE Transactions on Communications, 61(4): 1436-1449. https://doi.org/10.1109/TCOMM.2013.020413.110848

[4] Senger, S., Malik, P.K. (2022). A comprehensive survey of massive-MIMO based on 5G antennas. International Journal of RF and Microwave Computer-Aided Engineering, 32(12): e23496. https://doi.org/10.1002/mmce.23496

[5] Han, Y., Jin, S., Wen, C.K., Ma, X. (2020). Channel estimation for extremely large-scale massive MIMO systems. IEEE Wireless Communications Letters, 9(5): 633-637. https://doi.org/10.1109/LWC.2019.2963877

[6] Qi, C., Dong, P., Ma, W., Zhang, H., Zhang, Z., Li, G.Y. (2021). Acquisition of channel state information for mmWave massive MIMO: Traditional and machine learning-based approaches. Science China Information Sciences, 64(8): 181301. https://doi.org/10.1007/s11432-021-3247-2

[7] Li, Zheng, J., Zhang, J., Björnson, E., Ai, B. (2021). Impact of channel aging on cell-free massive MIMO over spatially correlated channels. IEEE Transactions on Wireless Communications, 20(10): 6451-6466. https://doi.org/10.1109/TWC.2021.3074421

[8] Chawla, A., Jagannatham, A.K. (2019). Spectral efficiency of very large multiuser MIMO systems for time-selective fading. In 2019 IEEE 89th Vehicular Technology Conference (VTC2019-Spring), Kuala Lumpur, Malaysia, pp. 1-5. https://doi.org/10.1109/VTCSpring.2019.8746439

[9] Shi, D., Wang, W., You, L., Song, X., Hong, Y., Gao, X., Fettweis, G. (2021). Deterministic pilot design and

channel estimation for downlink massive MIMO-OTFS systems in presence of the fractional Doppler. IEEE Transactions on Wireless Communications, 20(11): 7151-7165. https://doi.org/10.1109/TWC.2021.3081164

[10] Hou, H., Wang, Y., Zhu, Y., Yi, X., Wang, W., Slock, D. T., Jin, S. (2025). A tensor-structured approach to dynamic channel prediction for massive MIMO systems with temporal non-stationarity. IEEE Transactions on Wireless Communications, 25: 6869-6886. https://doi.org/10.1109/TWC.2025.3627432

[11] Chopra, R., Murthy, C.R., Appaiah, K. (2024). Adaptive data-aided time-varying channel tracking for massive MIMO systems. IEEE Transactions on Communications, 72(9): 5458-5472. https://doi.org/10.1109/TCOMM.2024.3386719

[12] Kashyap, S., Mollén, C., Björnson, E., Larsson, E.G. (2017). Performance analysis of (TDD) massive MIMO with Kalman channel prediction. In 2017 IEEE International Conference on Acoustics, Speech and Signal Processing (ICASSP), New Orleans, LA, USA, pp. 3554-3558. https://doi.org/10.1109/ICASSP.2017.7952818

[13] Sun, Y., Shen, H., Xu, W., Hu, N., Zhao, C. (2023). Robust MIMO detection with imperfect CSI: A neural network solution. IEEE Transactions on Communications, 71(10): 5877-5892. https://doi.org/10.1109/TCOMM.2023.3299974

[14] Feng, Z., Clerckx, B. (2023). Deep reinforcement learning for multi-user massive MIMO with channel aging. IEEE Transactions on Machine Learning in Communications and Networking, 1: 360-375. https://doi.org/10.1109/TMLCN.2023.3325299

[15] Wang, Y., Yi, X., Hou, H., Wang, W., Jin, S. (2024). Robust symbol-level precoding for massive MIMO communication under channel aging. IEEE Transactions on Wireless Communications, 23(9): 10864-10878. https://doi.org/10.1109/TWC.2024.3376796

[16] Ngo, H.Q., Tran, L.N., Duong, T.Q., Matthaiou, M., Larsson, E.G. (2017). On the total energy efficiency of cell-free massive MIMO. IEEE Transactions on Green Communications and Networking, 2(1): 25-39. https://doi.org/10.1109/TGCN.2017.2675713

[17] Deng, D., Li, X., Menon, V.G. (2021). Learning based MIMO communications with imperfect channel state information for Internet of Things. Multimedia Tools and Applications, 80(20): 31265-31276. https://doi.org/10.1007/s11042-020-10387-6

[18] Kim, H., Choi, J. (2019). Channel estimation for spatially/temporally correlated massive MIMO systems with one-bit ADCs. EURASIP Journal on Wireless Communications and Networking, 2019(1): 267. https://doi.org/10.1186/s13638-019-1587-x

[19] Lu, A.A., Gao, X., Zhong, W., Xiao, C., Meng, X. (2019). Robust transmission for massive MIMO downlink with imperfect CSI. IEEE Transactions on Communications, 67(8): 5362-5376. https://doi.org/10.1109/TCOMM.2019.2912383